**Supporting Information**

# Ground State Depletion Nanoscopy Resolves Semiconductor Nanowire Barcode Segments at Room Temperature

*Joanna Oracz,[†,‡] Karl Adolfsson,[§] Volker Westphal,[†] Czesław Radzewicz,[‡] Magnus T. Borgström,[§] Steffen J. Sahl,[†] Christelle N. Prinz[§] & Stefan W. Hell[†]*

[†]Department of NanoBiophotonics, Max Planck Institute for Biophysical Chemistry, 37077 Göttingen, Germany

[‡]Faculty of Physics, University of Warsaw, 02-093 Warsaw, Poland

[§]Division of Solid State Physics and NanoLund, Lund University, 22100 Lund, Sweden

**Table of Contents**

**Experimental setup**

Measurements were performed on a home-built microscopy system equipped with a commercial Ti:Sapphire oscillator (Mai Tai, Spectra Physics), a piezo scanner (NanoMax MAX312D, Melles Griot) and a high numerical aperture objective (NA 1.4, 100×, Leica). A schematic drawing of the setup is presented in Figure S1a. A doughnut-shaped excitation profile in the focal plane was generated by a helical phase plate (HPP, VPP-1a, Rochester Photonics). Confocal recordings were performed without the HPP. Nanowires were excited at ~700 nm by ~5 ps laser pulses stretched in a polarization-maintaining single-mode fiber. The pulse repetition rate was 80 MHz. Photoluminescence was filtered by bandpass/cut-off filters (AHF Analysentechnik, Semrock) and detected by a single-photon counting avalanche photodiode (APD, SPCM-AQR-13-FC, Perkin Elmer). In some experiments, the APD was replaced by a single-photon counting module with high temporal resolution (low dead time) (id100, idQuantique). Confocal detection was realized by a multimode fiber (M31LO3, Thorlabs) with ~1 Airy diameter. The photoluminescence lifetime was recorded with a time-correlated single-photon counting module (SPC-150, Becker & Hickl). The response function of the detection electronics (jitter) was measured by scattering of an ultrashort laser pulse (~128 fs) to be 40 ps (Figure 1d). Typical excitation powers for the recording of super-resolution GSD images varied from 0.5 mW to 7 mW. All powers stated were measured at the back aperture of the objective lens. Pixel dwell times were adjusted to be ~0.1-1 ms. All optical experiments were carried out at room temperature.

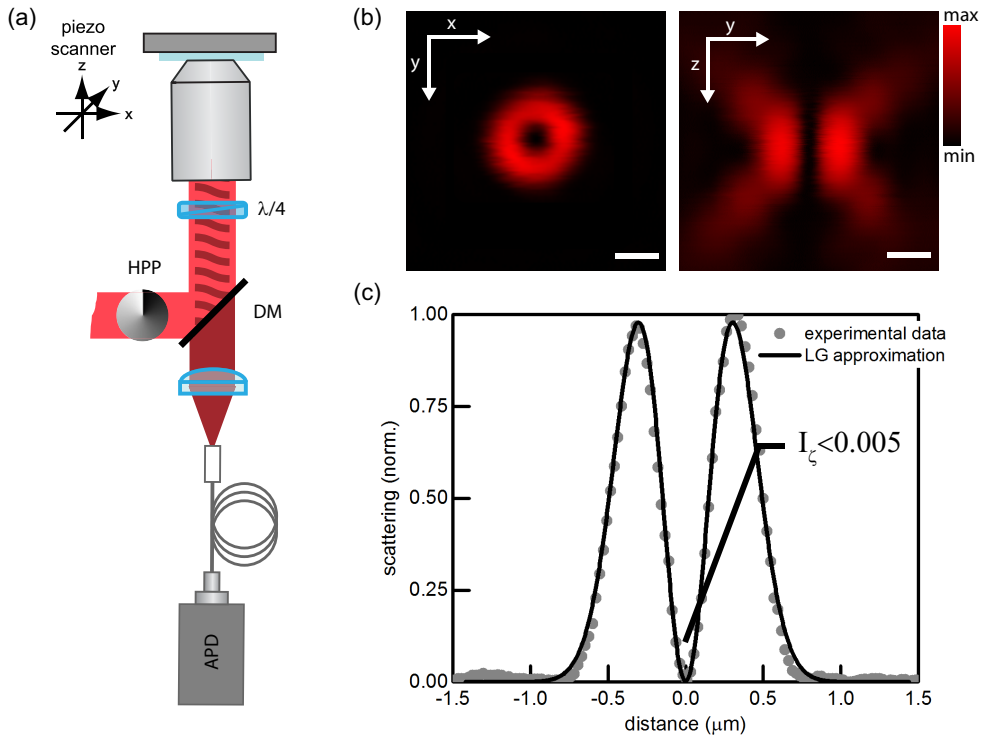


**Figure S1.** (a) Experimental setup for GSD nanoscopy (DM: dichroic mirror, APD: avalanche photodiode, HPP: helical phase plate, $\lambda/4$: quarter-wave plate). The scattered signal could be separately measured on a photomultiplier tube by reflection with a pellicle beamsplitter (path not shown). (b) Point spread function of the microscope, as measured by scattering of 80 nm gold beads in reflection. Scale bars: 500 nm. (c) Zero quality of the doughnut-shaped excitation beam measured to be $I_\zeta < 0.5\%$ (LG: Laguerre-Gaussian).

**Synthesis of GaP/GaInP barcode nanowires**

GaP/GaInP nanowires were synthesized by use of Au-particle assisted vapor liquid solid growth[1] in a commercial MOVPE system (Aixtron 200/4). Catalytic Au particles were deposited on GaP(111)B substrates by means of aerosol deposition[2], producing particles with diameter of 10, 20, 40 or 80 nm and at a surface density of 2 or 4 $\mu m^{-2}$. The substrate was then placed in the MOVPE reactor chamber. The epitaxial growth was preceded by a 10-min temperature annealing step at 650˚C with a constant $PH_3$ flow (molar fraction of $6.9\times10^{-3}$) in $H_2$ carrier gas (total flow of 13000 SCCM) to remove the native oxide from the GaP surface. The temperature was subsequently lowered to 440˚C and precursors for GaP were introduced into the reactor chamber, i.e. trimethylgallium (TMGa, at a molar fraction of $4.5\times10^{-5}$) and phosphine ($PH_3$, at a molar fraction

of $6.9\times10^{-3}$). Hydrogen chloride (HCl), which impedes undesirable radial growth, was also added at a molar fraction of $6.2\times10^{-5}$. Segments of GaInP were synthesized by introducing the precursor for indium, trimethylindium (TMIn at a molar fraction of $1.3\times10^{-5}$). The length and arrangement of GaP and GaInP segments were tuned by opening and closing the TMIn source at different time points. In our experiments, the GaInP growth time was varied between 1 s and 75 s, resulting in segments from ~50 nm to >200 nm in length. Nanowires with 1 and 4 GaInP segments were synthesized. The GaP growth time was varied between 5 s and 180 s, resulting in segment lengths between ~100 nm and 1.4 μm.

**Sample preparation**

The NWs substrate was first vertically placed in an Eppendorf tube filled with Milli-Q water and then sonicated for ~1 min to detach NWs from their substrate. Next, the dilute NWs suspension was spread on a coverslip (plasma-cleaned) and dried overnight or under a vacuum pump (drop-casting). A small drop of the microscope immersion oil used for imaging (Type B, Cargille) was added to a microscope object slide for index matching, and the coverslip put on top. After oil had spread out under the whole coverslip, the sample was sealed with nail polish.

**Mathematical image processing**

The present demonstration of PL GSD nanoscopy extracts high-resolution (sub-diffraction) information by preparing features in the "on" state everywhere except at and near the minimum of a doughnut-shaped excitation beam, resulting in "negative" images at raw data level. This drawback can in principle be overcome experimentally (by applying a second modulated laser beam, which excites non-saturated emitters, and a lock-in detection[3]), or by mathematical processing. The second option is easier to implement and does not necessitate slower recording. We therefore used two different methods: linear subtraction and Wiener deconvolution (Figure S2).

For the linear subtraction, we first applied a low-pass Gaussian filter to the original data set (Figure S2a) to remove high-resolution information from the image (Figure S2b). An image was then created by subtraction of original data from its low-resolution copy (Figure S2c: image b minus image a). In principle, a confocal image might be used as substitute for image b, but, due to potential movement of the piezo stage or any instability of the experimental system, the mathematical procedure is preferred. We implemented a Wiener deconvolution algorithm based on division of the raw data (image a) by the point spread function (PSF) of the GSD microscope

(Figure S2d) in the frequency domain. Deconvolution (Figure S2e) typically gave satisfactory results, however for small-diameter NWs (~20 nm) the image obtained by our Wiener deconvolution algorithm had substantial artifacts (Figure S2e).

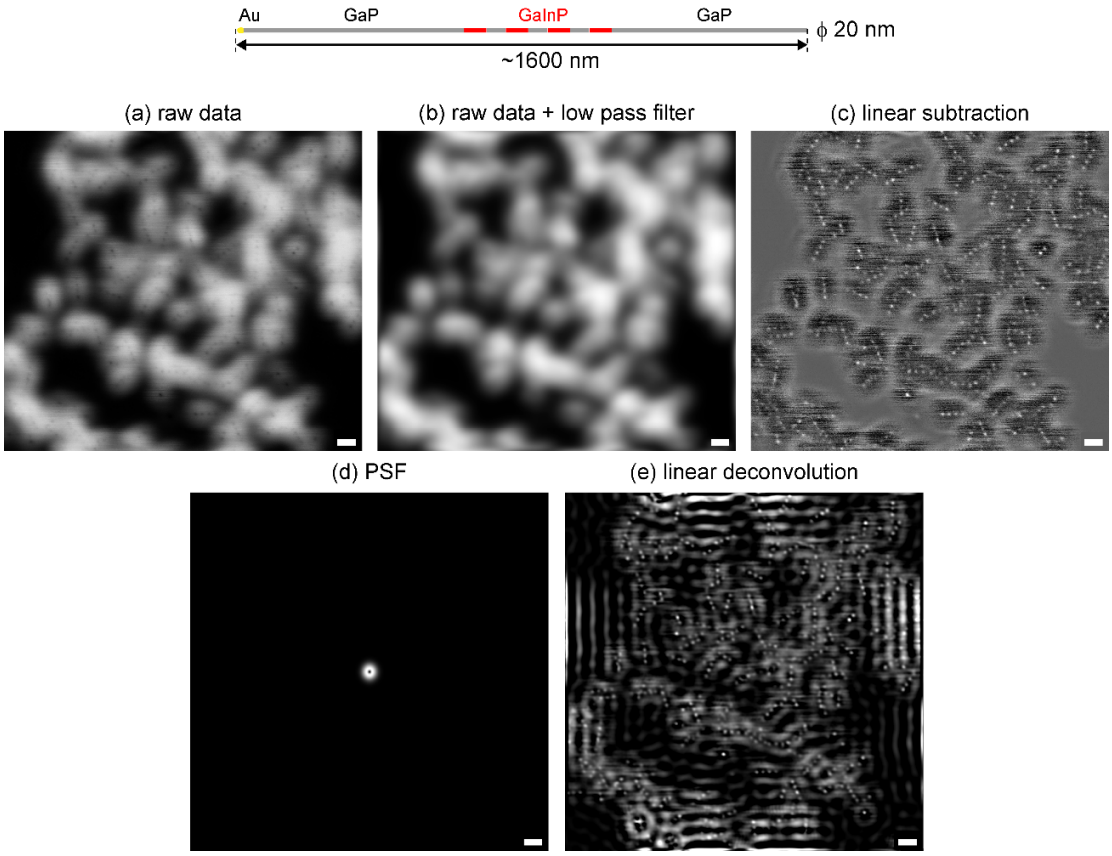


**Figure S2.** Image restoration. (a) Raw-data image of NW barcode ($\phi$=20 nm) with four luminescent segments. The excitation power was 4 mW. (b) Result of low-pass Gaussian filter applied to raw data. (c) Image created by linear subtraction (image b – image a). (d) Modeled point spread function for 4 mW. (e) Image resulting from Wiener deconvolution using the raw-data image (a) and the estimated PSF (d). All scale bars: 500 nm.

The PSF in GSD imaging is dependent on the emitter properties, and is difficult to assess experimentally for extended emitters. The GaInP PL segment size is comparable to the expected resolution, as estimated from the characterized saturation behavior (Figure 2a) and the PSF (Figure S1b). For this reason, we modeled an emitter response function $h_{GSD}$. We calculated the effective PSF using a non-saturated point spread function approximated by a Laguerre-Gaussian beam $h_{PSF}(r)$ (Figure S1c) and the experimentally measured saturation properties (Figure 2a):

$$h_{GSD}(r,P_{Exc}) = h_{PSF}(r) \otimes h_{obj}(\delta,P_{Exc})$$

$$h_{GSD}(r,P_{Exc}) \approx \left(1+\frac{P_S}{P_{Exc}\cdot 2.66(\frac{2r^2}{w_0^2}+\zeta)\exp(-\frac{2r^2}{w_0^2})}\right)^{-1}$$

where a point-like object is denoted by $h_{obj}$, the saturation average power is $P_S = 0.322$ mW, the average excitation power is $P_{Exc}$, the doughnut zero parameter is denoted by $\zeta = 0.001$, and the Gaussian beam width $w_0 = 430$ nm.

The effective PSF is a multiplication of $h_{GSD}$ with the confocal detection probability $h_{det}$. The detection probability was represented by a Gaussian distribution ($w_0 = 280$ nm), close to experimental conditions. The final effective PSF $h_{eff}$ then takes the form:

$$h_{eff}(r,P_{Exc}) = h_{GSD}(r,P_{Exc}) \times h_{det}(r).$$

Figure S3 displays a direct comparison between the simulated PSF and images of a single GaInP segment in a nanowire for four different average excitation powers.

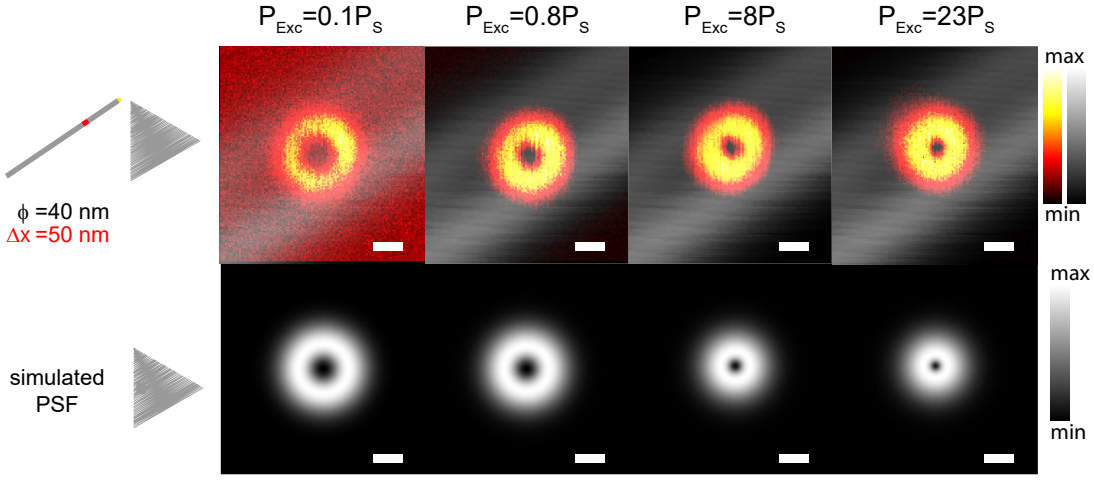


**Figure S3.** Comparison between raw-data images of a single small luminescent segment with diameter $\phi = 40$ nm and length $\Delta x = 50$ nm (top) and the predicted PSF of the GSD nanoscope (bottom) for different excitation powers. All scale bars: 200 nm.

**Results**

We compared the GSD nanoscopy results with standard confocal microscopy and scanning electron microscopy (SEM). The tables below report measurements for several NWs in a given field of view. Uncertainties were estimated as the standard deviation of reported measurements. In this study, we defined the contrast as $(I_{max} - I_{min}) / (I_{max} + I_{min})$.

Notation: $\Delta x_c$ – separation of adjacent maxima, $\Delta x$ – apparent segment length (FWHM), $\Delta y$– apparent segment width (FWHM).

NW #10188 J3 (Figure 3)

**Table S1.** Comparison of segment dimensions for NW #10188 J3 measured by confocal microscopy, GSD nanoscopy and electron microscopy.

| segment | **Confocal** | | **GSD raw data** | | **GSD deconvolved** | | **SEM** | |
|---|---|---|---|---|---|---|---|---|
| | Δx (nm) | Δy (nm) | Δx (nm) | Δy (nm) | Δx (nm) | Δy (nm) | Δx (nm) | Δy (nm) |
| GaInP | - | 388 ± 25 | 225 ± 14 | 76 ± 11 | 212 ± 22 | 73 ± 9 | 233 ± 39 | 25 ± 1 |
| GaP | - | | 162 ± 20 | | 174 ± 17 | | 164 ± 21 | 25 ± 1 |

Contrast along NW axis (at the middle segments): 0.13±0.01
Contrast across NW axis: 0.10±0.02

NW #9609 D3 (Figure 4)

**Table S2.** Comparison of segment dimensions for NW #9609 D3 measured by GSD nanoscopy and electron microscopy.

| segment | **GSD raw data** | | **GSD deconvolved data** | | | **SEM** | | |
|---|---|---|---|---|---|---|---|---|
| | $\Delta x_c$ (nm) | Δy (nm) | $\Delta x_c$ (nm) | Δx (nm) | Δy (nm) | $\Delta x_c$ (nm) | Δx (nm) | Δy (nm) |
| GaInP | 112 ± 13 | 84 ± 12 | 116 ± 6 | 66 ± 10 | 66 ± 6 | 114 ± 5 | 64 ± 15 | 43 ± 3 |

Contrast along NW axis (at the middle segments): 0.10±0.03
Contrast across NW axis: 0.21±0.02 to 0.07±0.03

NW #9607 A3 (Figure 5)

**Table S3.** Comparison of segment dimensions for NW #9607 A3 measured by GSD nanoscopy and electron microscopy.

| segment | **GSD raw data** | | | **GSD deconvolved data** | | | **SEM** | | |
|---|---|---|---|---|---|---|---|---|---|
| | $\Delta x_c$ (nm) | Δx (nm) | Δy (nm) | $\Delta x_c$ (nm) | Δx (nm) | Δy (nm) | $\Delta x_c$ (nm) | Δx (nm) | Δy (nm) |
| GaInP | 147 ± 14 | 69 ± 6 | 74 ± 12 | 146 ± 8 | 63 ± 13 | 62 ± 9 | 145 ± 4 | 50 ± 9 | 53 ± 2 |

Contrast along NW axis (at the middle segments): 0.14±0.01
Contrast across NW axis: 0.17±0.04

NW #10476 B1 (Figure S2)

**Table S4.** Separation of adjacent maxima and segment dimensions, as measured by GSD nanoscopy for NW #10476 B1.

| GSD raw data | | | | |
|---|---|---|---|---|
| segment | $\Delta x_c$ | segment | $\Delta x$ (nm) | $\Delta y$ (nm) |
| 1st-2nd GaInP | 164±9 | 1st GaInP | 72±10 | 67±12 |
| 2nd-3rd GaInP | 181±6 | 2nd GaInP | 74±12 | |
| 3rd-4th GaInP | 184±8 | 3rd GaInP | 73±19 | |
| | | 4th GaInP | 85±24 | |

**Limitations of direct subdiffraction imaging with GSD (resolution and contrast)**

The resolution enhancement is limited by several factors. One of them is the quality of the doughnut zero, which can influence the image contrast. We found that the non-zero intensity at the minimum (in our case $\zeta = 0.001$) only slightly influenced the contrast at applicable power levels (<20% reduction). The predicted resolution and contrast for a point-like luminescent segment (1×1 nm$^2$), calculated for the saturation properties and the analytical PSF (both informed by measurement), is presented in Figure S4.

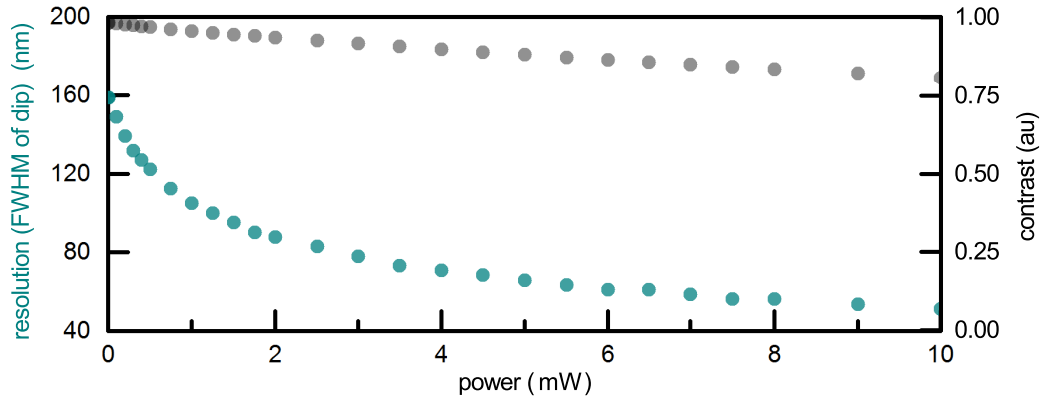


**Figure S4.** Resolution and contrast simulated for a point-like photoluminescent segment (1×1 nm$^2$). The quality of the doughnut zero was $\zeta = 0.001$.

A 66 nm spatial resolution can be obtained for excitation power $P_{Exc} = 5$ mW with meager contrast reduction by 10%. However, significant reductions of the contrast are related to the finite

size of the PL segments and/or multiple segments spaced within the diffraction limit (Figure 4h,i). In this case, PL of nearby excitons lowers the registered intensity dip. In Figure 4h, we show the contrast reduction as a function of PL segment length for different nanowire diameters $\phi$ (excitation power 5 mW). For a single luminescent segment with 20 nm diameter, the image contrast was reduced from 0.8 to 0.2 by increasing the GaInP length from 20 nm to 200 nm. Not only the segment length but also the spacing between several emissive segments influenced the depth of observed dips. The contrast as function of the separation (spacer length) between three adjacent luminescent segments with diameter and length both equal 20 nm is shown in Figure 4i. Separation smaller than the resolution (~60 nm) leads to indistinguishable segments and was not taken into account. For a separation close to the resolution, the contrast (simulated) has the lowest value ~0.16; increases in separation lead to nearly linearly increased contrast (Figure 4i).

The highest contrast can be obtained for the smallest luminescent objects at the expense of signal (which scales as the volume, i.e., number of electrons). As nanowires are exceptionally bright, we decreased both the diameter and the length of luminescent segments. However, small NWs (diameter <20 nm) exhibited strong PL intermittency, which makes GSD imaging impracticable (Figure S5). When NW luminescent segment size became comparable to the (bulk) exciton radius (for a $Ga_xIn_{1-x}P$ exciton the Bohr radius is ~4.2-8.6 nm), we observed significant fluctuations in emitted PL. Currently, these fluctuations are most often explained as induced by light charging of the semiconductor material, which then cannot emit light. Unneutralized charge is created by photoexcited carriers trapped in acceptor-like surface states, and eventually recombines via a non-radiative Auger-like mechanism. This charging effectively quenches emission until the semiconductor is re-neutralized. The nature of PL fluctuations is still not fully understood[4].

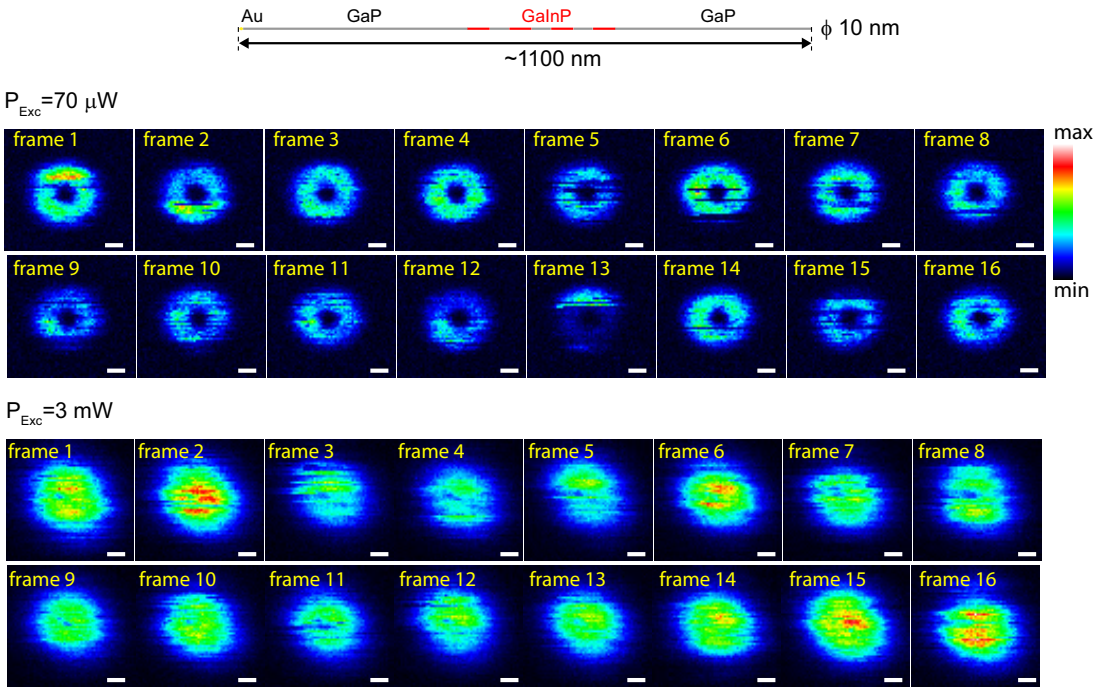


**Figure S5.** Photoluminescence of a single NW ($\phi$ = 10 nm) with four PL segments. An increased photoluminescence intermittency was observed due to the small diameter of the NW. The excitation power was 70 μW (top) and 3000 μW (bottom), the dwell time 1 ms. The photoluminescence segments became indistinguishable due to the strong signal fluctuations, which masked the expected signal dips. All scale bars: 200 nm.

A practical limit of resolution enhancement is related to permanent loss of PL from the emitter structure (Figure S6). Such damage eventually occurs after applying a high-power excitation beam and manifests as significantly lower PL signal and, very often, suddenly increased contrast of the recorded image. This contrast increase is likely due to reduction of the emissive segment volume. This observation is supported by changes in the scattering profile before and after photoluminescence decrease (Figure S6d). For a single NW, the threshold for permanent signal loss varied from 3 to 7 mW, depending on the NWs. The mechanisms of PL decrease are beyond the scope of this article.

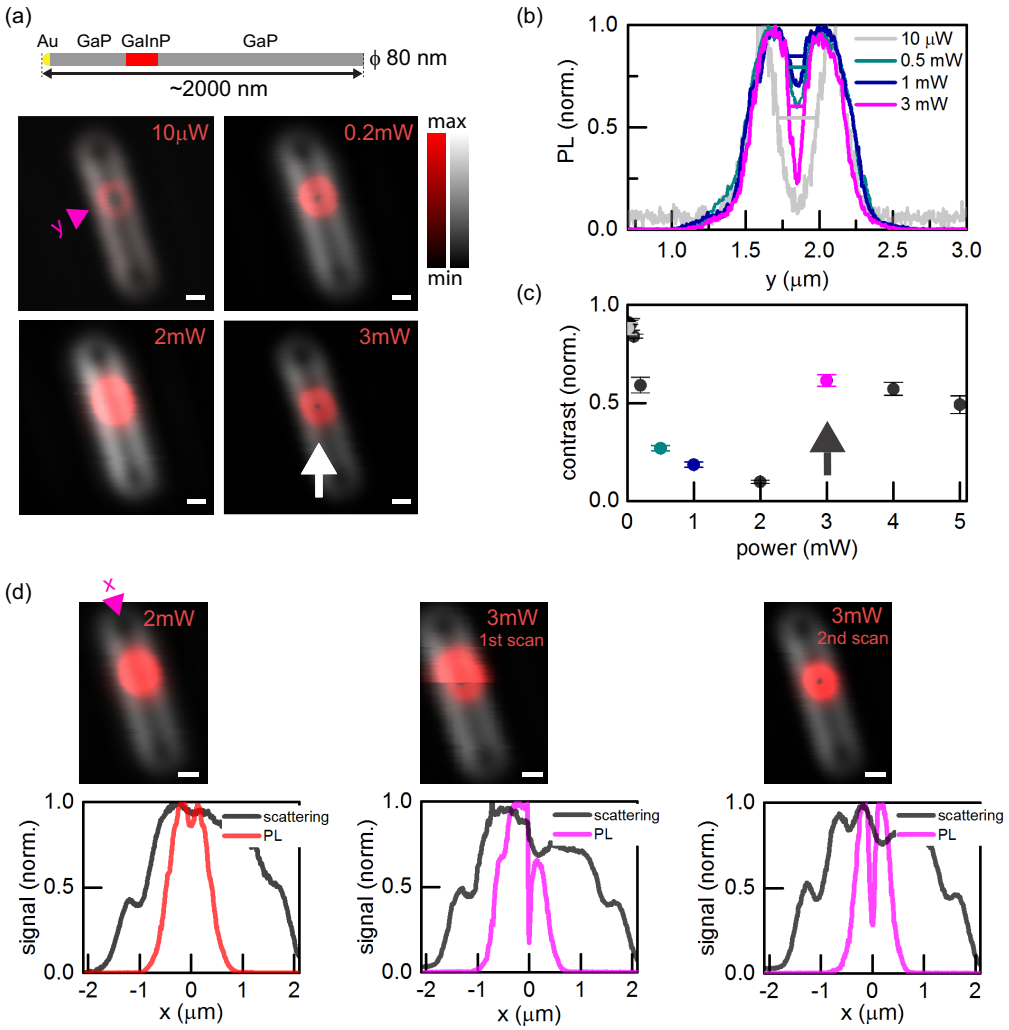


**Figure S6.** (a) Scattering (gray) and photoluminescence (red) of a single NW ($\phi$ = 80 nm) with a single GaInP segment. (b) Photoluminescence intensity profiles show resolution changes as a function of the excitation power for the same NW. The resolution was defined as the full-width at half-maximum (FWHM) of the signal dip to minimum. (c) Contrast for data in b. The arrow indicates the abrupt reduction of photoluminescence. (d) The same NW imaged with GSD (successive scans). The decrease in photoluminescence was accompanied by a significant increase in the contrast of the image, which suggests a volume reduction of the luminescent segment. All scale bars: 400 nm.

**Specifications of NWs**

NW #9030 A8 (Figure 2, Figure S3)

**Table S5.** Geometry of NW #9030 A8 based on the growth time.

| NW density | gold bead | growth properties | | | total length |
|---|---|---|---|---|---|
| | | 2 min | 5 s | 2 min | |
| | | GaP | GaInP | GaP | |
| 4/μm² | 40 nm | ~1.1μm | <100 nm | ~0.9μm | ~2 μm |

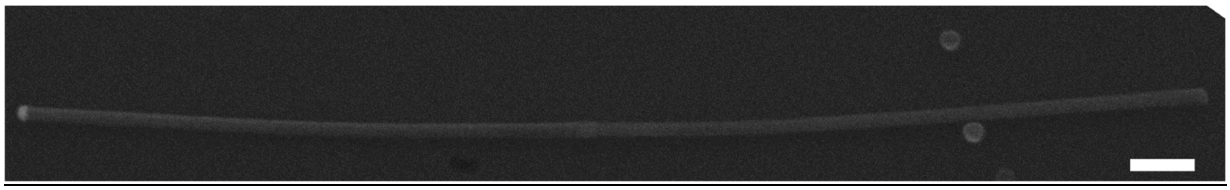

**Figure S7.** Example SEM image of barcode NW #9030 A8. Measured GaInP segment length and width both ~50 nm. Scale bar: 200 nm.

NW #10188 J3 (Figure 3)

**Table S6.** Geometry of NW #10188 J3 deduced from growth time.

| NW density | gold bead | growth properties | | | | | | | | | total length |
|---|---|---|---|---|---|---|---|---|---|---|---|
| | | 2 min | 5 s | 10 s | 5 s | 10 s | 5 s | 10 s | 5 s | 1min | |
| | | GaP | GaInP | GaP | GaInP | GaP | GaInP | GaP | GaInP | GaP | |
| 2/μm² | 20nm | ~1.4μm | ~150nm | ~100nm | ~150nm | ~100nm | ~150nm | ~100nm | ~150nm | ~1.2μm | ~3.5 μm |

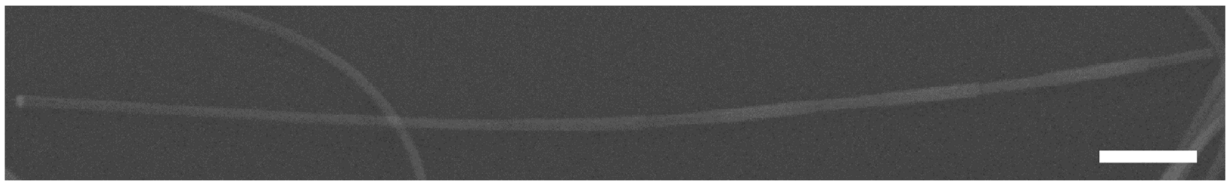

**Figure S8.** Example SEM image of barcode NW #10188 J3. Measured GaInP/GaP segment lengths equal $233 \pm 39 / 164 \pm 21$ nm respectively, with diameter $25 \pm 2$ nm. Scale bar: 200 nm.

NW #9609 D3 (Figure 4)

**Table S7.** Geometry of NW #9609 D3 deduced from growth time.

| NW density | gold bead ϕ | growth properties | | | | | | | | | total length |
|---|---|---|---|---|---|---|---|---|---|---|---|
| | | 2 min | 5 s | 7 s | 5 s | 7 s | 5 s | 7 s | 5 s | 1min | |
| | | GaP | GaInP | GaP | GaInP | GaP | GaInP | GaP | GaInP | GaP | |
| 2/μm² | 40nm | ~0.4μm | ~70nm | ~70nm | ~70nm | ~70nm | ~70nm | ~70nm | ~70nm | ~0.5μm | ~ 1.4μm |

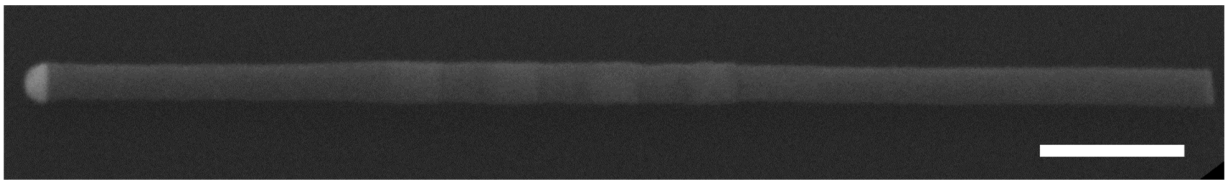

**Figure S9.** Example SEM image of barcode NW #9609 D3. Measured GaInP segment length $64 \pm 15$ nm, with $114 \pm 5$ nm separation between the adjacent maxima. NW diameter retrieved by SEM: $43 \pm 3$ nm. Scale bar: 200 nm.

NW #9607 A3 (Figure 5)

**Table S8.** Geometry of NW #9607 A3 deduced from growth time.

| NW density | gold bead ϕ | growth properties | | | | | | | | | total length |
|---|---|---|---|---|---|---|---|---|---|---|---|
| | | 2 min | 5 s | 10 s | 5 s | 10 s | 5 s | 10 s | 5 s | 1min | |
| | | GaP | GaInP | GaP | GaInP | GaP | GaInP | GaP | GaInP | GaP | |
| 2/μm² | 40nm | ~500nm | ~50nm | ~0.1μm | ~50nm | ~0.1μm | ~50nm | ~0.1μm | ~50nm | ~500nm | ~1.5 μm |

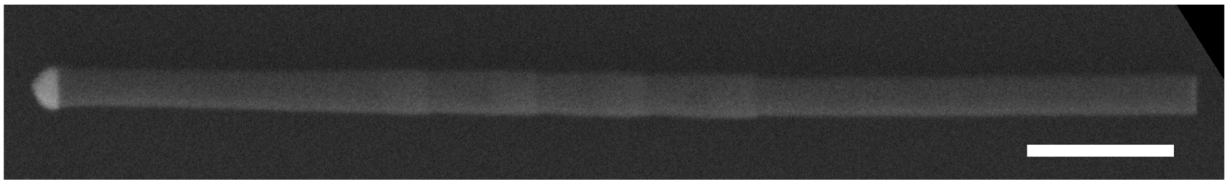

**Figure S10.** Example SEM image of barcode nanowire #9607 A3. Measured GaInP segment length $50 \pm 9$ nm, with $145 \pm 4$ nm separation between the adjacent maxima. NW diameter retrieved by SEM: $53 \pm 2$ nm. Scale bar: 200 nm.

NW #10476 B1 (Figure S2)

**Table S9.** Geometry of NW #10476 B1 deduced from growth time.

| NW density | gold bead ϕ | growth properties | | | | | | | | | total length |
|---|---|---|---|---|---|---|---|---|---|---|---|
| | | 2 min | 5 s | 12 s | 5 s | 10 s | 5 s | 8 s | 5 s | 1min | |
| | | GaP | GaInP | GaP | GaInP | GaP | GaInP | GaP | GaInP | GaP | |
| 2/μm² | 20nm | ~500nm | ~50nm | ~90nm | ~50nm | ~90nm | ~50nm | ~90nm | ~50nm | ~600nm | ~ 1.6 μm |

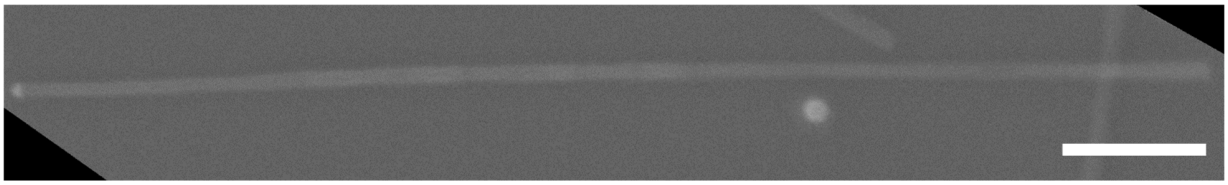

**Figure S11.** SEM image of barcode nanowire #10476 B1. Scale bar: 200 nm.

NW #10474 A6 (Figure S5)

**Table S10.** Geometry of NW #10474 with growth times for individual segments.

| NW density | gold bead ϕ | growth properties | | | | | | | | | total length |
|---|---|---|---|---|---|---|---|---|---|---|---|
| | | 2 min | 5 s | 10 s | 5 s | 8 s | 5 s | 5 s | 5 s | 1min | |
| | | GaP | GaInP | GaP | GaInP | GaP | GaInP | GaP | GaInP | GaP | |
| 4/μm$^2$ | 10nm | * | * | * | * | * | * | * | * | * | ~ 1.1 μm |

(*) difficult to estimate segment lengths

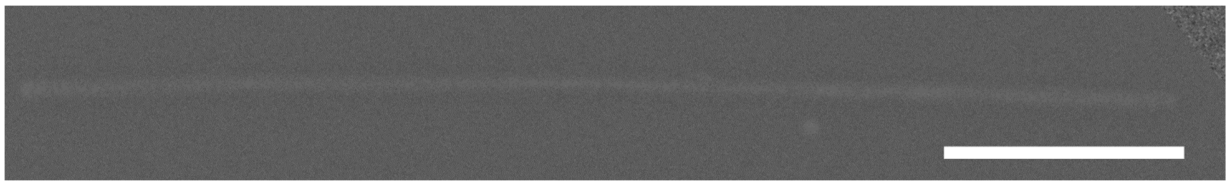

**Figure S12.** SEM image of barcode nanowire #10474 A6. Scale bar: 200 nm.

NW #7816 (Figure S6)

**Table S11.** Geometry of NW #7816 deduced from growth time.

| NW density | gold bead ϕ | growth properties | | | total length |
|---|---|---|---|---|---|
| | | 3 min | 1+15 s | 1.5 min | |
| | | GaP | GaInP | GaP | |
| 2/μm$^2$ | 80nm | ~1.3μm | ~200nm | ~0.5μm | ~2 μm |

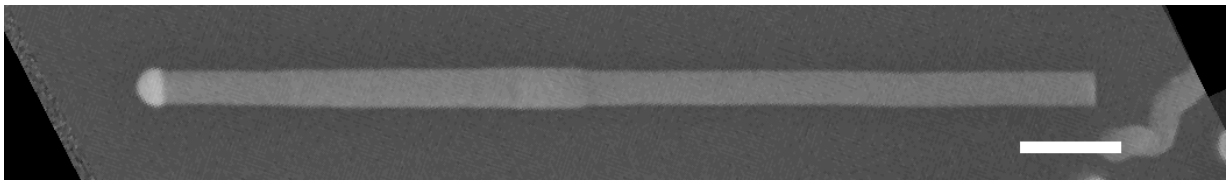

**Figure S13.** SEM image of barcode nanowire #7816. Scale bar: 200 nm.

**Lookup tables (color scales)**

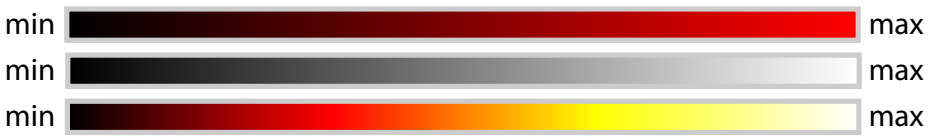


**Figure S14.** Color scales used in Figures 2-5.

## References


1. Wagner, R. S.; Ellis, W. C. *Appl. Phys. Lett.* **1964,** 4, (5), 89-90.
2. Magnusson, M. H.; Deppert, K.; Malm, J.-O.; Bovin, J.-O.; Samuelson, L. *Nanostruct. Mater.* **1999,** 12, (1–4), 45-48.
3. Rittweger, E.; Wildanger, D.; Hell, S. W. *EPL* **2009,** 86, (1), 14001.
4. Frantsuzov, P.; Kuno, M.; Janko, B.; Marcus, R. A. *Nat. Phys.* **2008,** 4, (5), 519-522.